International Journal of Applied Earth Observation and Geoinformation 123 (2023) 103484

Contents lists available at ScienceDirect

International Journal of Applied Earth Observation and Geoinformation

journal homepage: www.elsevier.com/locate/jag

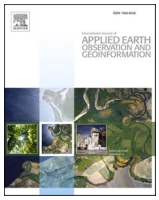

# Spatial heterogeneity of uncertainties in daily satellite nighttime light time series

Xiaoyue Tan [a], Ruilin Chen [b], Xiaolin Zhu [a,c,*], Xi Li [d], Jin Chen [b], Man Sing Wong [a,e], Shuai Xu [a], Yi Nam Xu [a]

[a] Department of Land Surveying and Geo-Informatics, The Hong Kong Polytechnic University, Hong Kong, China
[b] State Key Laboratory of Remote Sensing Science, Faculty of Geographical Science, Beijing Normal University, Beijing 100875, China
[c] Otto Poon Charitable Foundation Smart Cities Research Institute, The Hong Kong Polytechnic University, Hong Kong, China
[d] State Key Laboratory of Information Engineering in Surveying, Mapping and Remote Sensing, Wuhan University, Wuhan 430079, China
[e] Research Institute for Land and Space, The Hong Kong Polytechnic University, Hong Kong, China

ARTICLE INFO

*Keywords:*
Nighttime light
VIIRS DNB
Black Marble
Artificial light radiance
Time-series variation

ABSTRACT

Remotely sensed light imagery provides a unique perspective for high-frequency human activity monitoring. NASA has developed the Black Marble, a daily nighttime light (NTL) product from the Visible Infrared Imaging Radiometer Suite (VIIRS) nighttime images by correcting environmental effects (i.e., atmospheric, lunar, and stray light effects). However, variation and uncertainty remain in the daily lunar-BRDF corrected NTL product and hinder its quantitative applications. To better understand the uncertainty across multiple spatial and temporal scales, this study proposed a spatial–temporal hierarchical analysis strategy to separate uncertainties from different sources, and evaluated the effects of multiple factors on daily NTL time series. The experiments conducted on two populous regions show that: (1) The daily NTL in Northern America has variations up to 50% of the annual average, which is stronger than in East Asia, with variations up to 25%. (2) The variation in seasonality is stronger in Northern America, whereas the variation related to day-to-day changing factors is stronger in East Asia. (3) Generalized linear models are built to capture the relationship between daily NTL and influential factors in each grid, revealing that approximately 25%~50% of the daily variations can be explained by environmental factors, observational factors, and seasonality. (4) Environmental factors and observational conditions show spatially varying impacts on NTL. Specifically, aerosol exhibit opposite impacts on rural and urban areas; significant impacts of moonlight are mainly distributed in rural areas; the impact of satellite viewing angle is less pronounced and frequent in East Asian cities compared to those in North America. This research revealed the essential knowledge about variations of satellite-derived NTL and will benefit the processing and utilization of daily NTL products.

## 1. Introduction

Remotely sensed light imagery offers a unique perspective depicting human activities. Since the 1970s, several satellite sensors have been launched to detect nighttime lights (NTL), including the Defense Meteorological Satellite Program-Operational Linescan System (DMSP-OLS) (Elvidge et al., 1997), Visible Infrared Imaging Radiometer Suite (VIIRS) (Miller et al., 2012b) onboard Suomi-NPP satellite and NOAA-20, Luojia-01 (Li et al., 2018; Ou et al., 2019), Jilin1-03B (Zheng et al., 2018), SDGSAT-1 (Guo et al., 2023) and small satellites such as Yangwang-1 (Zhu et al., 2022). The released NTL datasets have yielded valuable insights into various fields and applications (Kyba et al., 2017; Levin et al., 2020; Zhao et al., 2019). Furthermore, continuous global daily NTL products released by the Earth Observation Group (EOG) (Elvidge et al., 2017), NASA's Black Marble nighttime lights product suite (VNP46) (Román et al., 2018), and NOAA-20 VIIRS daily NTL data are increasingly utilized due to their unique capabilities in capturing rapid human activities, such as cultural patterns on holidays (Román and Stokes, 2015), power outages (Cao et al., 2013; Elvidge et al., 2020b), and the economy in COVID-19 pandemic (Elvidge et al., 2020a; Xu et al., 2021; Zhao et al., 2022), as well as dynamics in natural systems including natural disasters (Zhao et al., 2018), snow cover (Huang et al.,

* Corresponding author at: The Hong Kong Polytechnic University, Room ZS621, Block Z, 181 Chatham Road South, Kowloon, Hong Kong.
*E-mail address:* xiaolin.zhu@polyu.edu.hk (X. Zhu).

https://doi.org/10.1016/j.jag.2023.103484
Received 14 May 2023; Received in revised form 1 August 2023; Accepted 4 September 2023
Available online 8 September 2023

2022), nocturnal fire (Polivka et al., 2016; Wang et al., 2020) and air conditions (Wang et al., 2016; Zhang et al., 2019).

NTL observation from satellites is susceptible to various factors (e.g., acquisition conditions, observational geometry, surface environments) that lead to undesired noise, thus limiting its application, especially for daily NTL time series (Levin et al., 2020). A great deal of effort has been put into mitigating artifacts caused by environmental factors for producing high-quality NTL data (Cao et al., 2013; Liao et al., 2013; Miller et al., 2012a; Miller and Turner, 2009; Román and Stokes, 2015). Currently, NASA's Black Marble daily nighttime lights product suite (VNP46) provides the only public-access daily lunar BRDF (Bidirectional Reflectance Distribution Function) adjusted NTL dataset (Román et al., 2018). Although NASA's Black Marble algorithm includes corrections for atmospheric, terrain, lunar BRDF, thermal, and stray light effects, a recent assessment study pointed out that the daily Black Marble corrected NTL data still has non-negligible uncertainties (Wang et al., 2021). Besides, another research suggests that the Black Marble corrected NTL data has uncertainties across different spatial and temporal scales (Zheng et al., 2022).

A comprehensive assessment of uncertainties in daily nighttime light (NTL) time series is crucial for several reasons. Firstly, gaining a comprehensive understanding of the overall uncertainties in NTL time series is crucial for end users, as accurate interpretation of daily NTL variations is vital in various applications (Levin et al., 2020). Moreover, it is important to note that the intensity and major influential factors of uncertainties may vary across different spatial locations, yet these variations remain unclear. However, previous research has primarily conducted evaluations on selected sites or cities (Wang et al., 2021), resulting in a lack of comprehensive evaluations and comparisons of the spatiotemporal patterns of uncertainty in larger regions. Secondly, it is important to highlight that previous studies investigating environmental impacts in large regions have predominantly relied on monthly composited NTL datasets (Levin, 2017; Yuan et al., 2022). However, these temporal composite data ignored daily-changing factors and thereby could fail to capture high-frequency variations in NTL time series. Thirdly, it is crucial to acquire knowledge regarding the impact of environmental factors on daily lunar BRDF-corrected NTL images for future research and application, as the corrected NTL time series are more suitable for practical use. Although certain studies have demonstrated the influence of environmental factors on top-of-atmosphere (TOA) nighttime radiance (Román et al., 2018), it is worth noting that these impacts may have been attenuated or altered during the correction process.

To fill the above research gaps, this research investigates the variations in Black Marble corrected daily NTL and its response to external factors. Specifically, the following research questions will be addressed: (1) What patterns of daily NTL variation are at multiple spatial and temporal scales. (2) What are the differences in intensity and spatial extent of uncertainty from different sources. (3) What is the contribution of environmental factors and observation conditions to daily NTL uncertainty. This research provides new insights into the uncertainty of satellite-derived NTL radiance and sheds light on the distinction between NTL variations and actual changes to artificial light.

## 2. Study material

### 2.1. Study area

Two regions from Northern America and East Asia were selected as the research areas (Fig. 1). Numerous cities and towns are located in these two regions. They are home to hundreds of millions of people, making them among the most popular study areas in nighttime light-related research in recent years (Bennett and Smith, 2017). Furthermore, these two regions cover a variety of natural and human environments and thus are ideal for examining the spatiotemporal variation in NTL. For instance, the two study areas cross low to high latitudes (20°N – 60°N), various landforms (including mountains, hills, plateaus, and plains), and different climate zones. Settlement areas range from small villages to large megacities of ten million people, encompassing different urban structures (Li et al., 2020a) and sociocultural environments that may affect lighting patterns (Román and Stokes, 2015).

### 2.2. Data

#### 2.2.1. NTL radiance data

NTL radiance data used in this research are extracted from NASA's daily Black Marble products suite (VNP46, Collection V001). These products are derived from original images acquired by the Day/Night Band (DNB) sensor of VIIRS, on board the Suomi-NPP and Joint Polar Satellite System (JPSS) satellite platforms. The DNB sensor is designed for observing nocturnal visible and near-infrared light, providing global daily measurements at a spatial resolution of 500 m (Elvidge et al.,

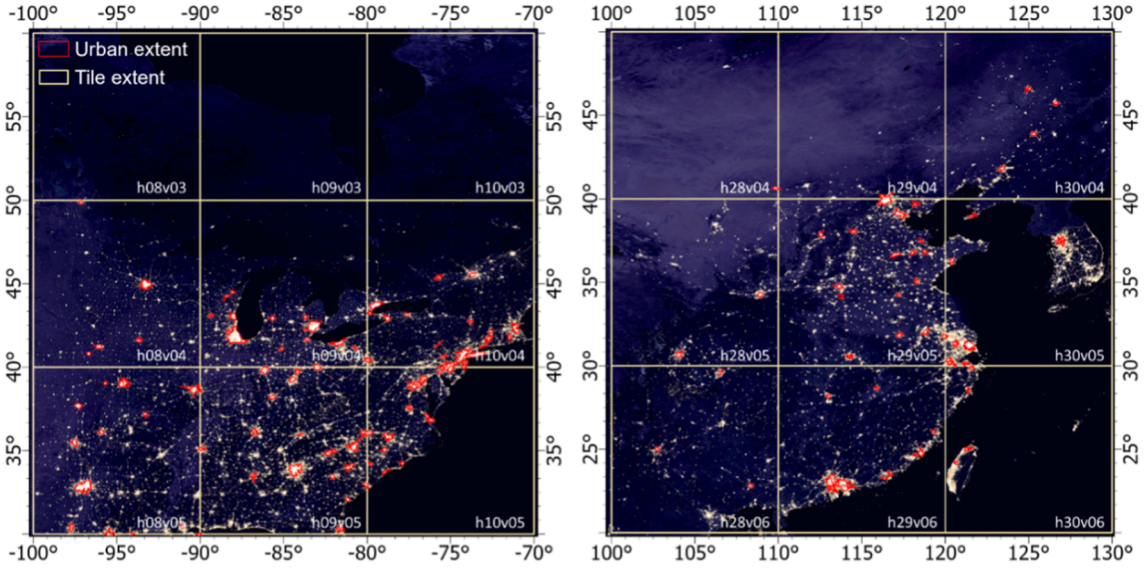


**Fig. 1.** Study areas in Northern America and East Asia. Each site covers 9 Black Marble tiles (yellow square grids). Urban area boundaries are shown in red (80 urban samples in the Northern America site and 67 in the East Asia site). (For interpretation of the references to color in this figure legend, the reader is referred to the web version of this article.)

2017). The Black Marble product suite offers daily and temporal composited NTL products from 2012 onwards. VNP46A1 provides the daily at-sensor TOA NTL product. VNP46A2 refines this data by applying corrections for lunar BRDF, cloud, terrain, atmospheric, airglow, stray light, etc. The corresponding mandatory quality flag band in VNP46A2 can be used to filter out pixels contaminated by clouds, snow, or labeled as non-valid retrievals. VNP46A3 offers multiple types of monthly compositions, differs based on their respective zenith angle categories (near-nadir, off-nadir, and all angles) and snow status (snow-covered and snow-free). Monthly snow-free composited radiance band from VNP46A3 was used to explore the seasonality of NTL. According to the detection limit of NASA's Black Marble product suite, grid cells with radiances<0.5 nW/cm$^2$/sr were discarded as background noise (Román et al., 2018). To reduce geometric effects due to the spatial mismatch (Wang et al., 2021), NTL radiance images were resampled to a spatial resolution of 0.05° by spatial averaging by calculating average spatial. During this process, only high-quality pixels, as indicated in the quality flag layer, are utilized. Resampled grid cells are included in subsequent analyses only when over half of their corresponding original pixels labeled as high quality.

#### 2.2.2. Environmental factors observational conditions data

Environmental factors that may affect the satellite-derived NTL include vegetation, aerosol, ground-level particulate matter, and moonlight. Daily AOD at 550 nm was extracted from MODIS Terra and Aqua combined Multi-angle Implementation of Atmospheric Correction (MAIAC) Land Aerosol Optical Depth dataset (MCD19A2, version 6). Day/Night Band (DNB) Lunar Irradiance band in VNP46A2 was used to explore the impact of moonlight on NTL observations. The viewing zenith angle (VZA) was extracted from VNP46A1 to examine NTL variation caused by satellite viewing angles. Satellite overpass time was extracted from the Time UTC band in VNP46A1 as a control variable in NTL radiance modeling.

#### 2.2.3. Urban boundary data

This study used satellite images-driven urban boundaries to assist in the statistics and analysis of city-level NTL variation. Global urban boundaries in several representative years are provided by the 30 m Global Artificial Impervious Area (GAIA) dataset (Li et al., 2020b), available at https://data.starcloud.pcl.ac.cn/. Urban boundaries in 2010 were used to facilitate the extraction of city-level NTL variation. Using the boundaries in earlier years makes it possible to avoid areas with large interannual NTL changes due to urban extension. All urban polygons with an area greater than 250 km$^2$ were analyzed (Fig. 1). Totally 80 cities and 67 cities were selected from the Northern America and East Asia sites, respectively.

## 3. Methodology

This research proposed two modules to answer the three questions (Fig. 2). The first module is a spatial–temporal hierarchical analysis proposed to quantify daily NTL variation. Four distinct types of time series primarily influenced by specific factors were segregated and scrutinized at four different spatial scales. This module aims to gain a comprehensive understanding of research questions 1 and 2 (Q1 and Q2 in Fig. 2). In the second module, generalized linear models (GLMs) is employed to establish the relationship between daily changes in NTL and environmental factors as well as observational conditions on grid cell level. The GLM was chosen for its ability to establish relationships between the response variable and multiple independent variables through a link function, enabling the capture of underlying non-linear relationships. Furthermore, GLM allows for gain clear interpretations of multiple variables' impacts on the response variable, i.e., marginal effects. The marginal effects of these factors are calculated based on these GLMs to answer Q3 in Fig. 2.

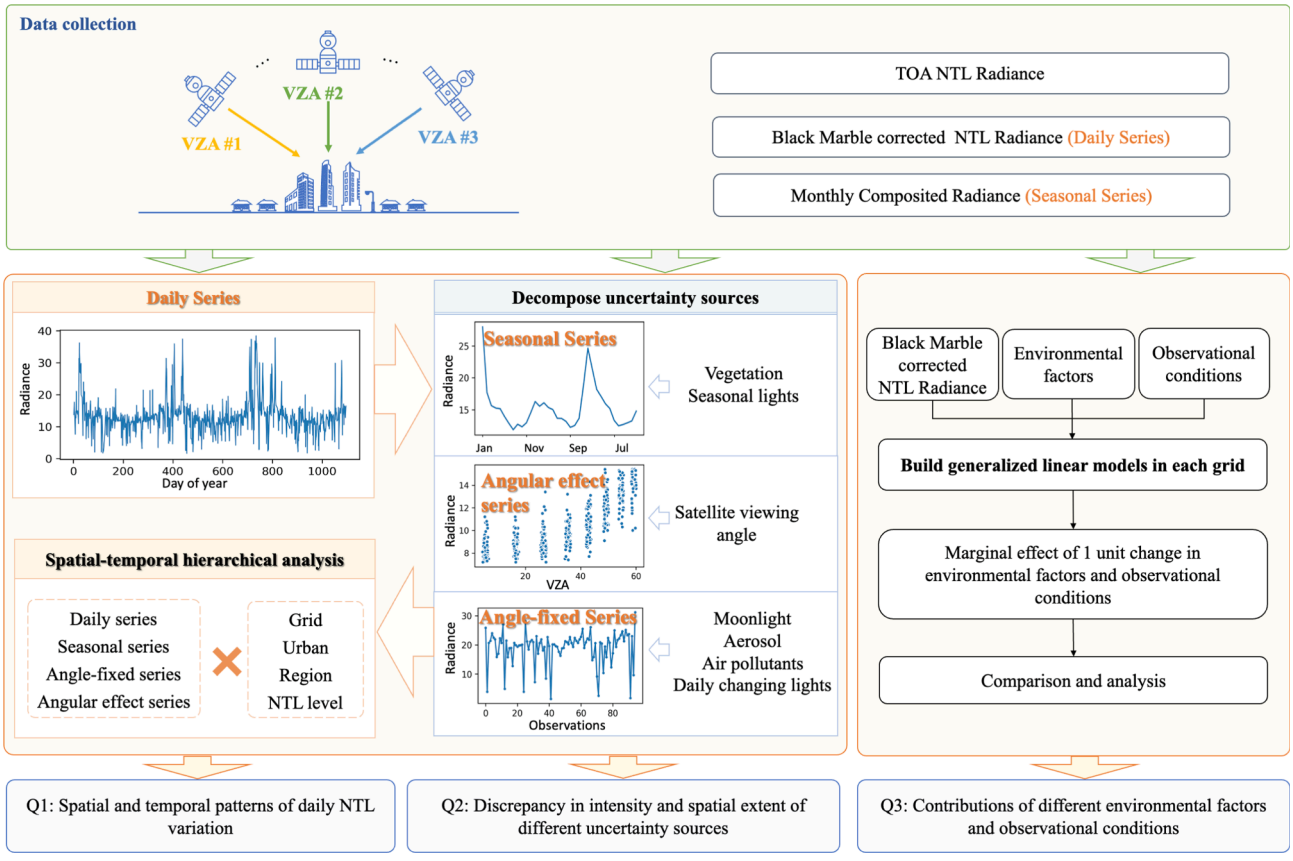


**Fig. 2.** Illustrative diagram of the research methodology.

### 3.1. Quantifying NTL variation across various spatial–temporal scales

This research proposed a spatial–temporal hierarchical analysis strategy to evaluate the NTL variation across various spatial–temporal scales. By slicing the NTL time series differently, four types of time series were generated, in which certain types of factors dominate the variation:

- **Daily series:** directly extracted from daily NTL, including the observation of each day in the research period. Daily series is affected by all factors considered in this research.
- **Seasonal series:** directly extracted from near-nadir monthly composited NTL radiance products, which eliminates the influence of satellite viewing angle and daily changing environmental factors such as atmospheric conditions and moonlight. Seasonal series can thus capture seasonal variations caused by seasonal environmental factors such as vegetation (Zheng et al., 2022).
- **Angle-fixed series:** extracted from daily NTL based on the VZA of each observation. As shown in Fig. 3, VZA was into six bins of 10-degree intervals (0°–10°, 10°–20°, 20°–30°, 30°–40°, 40°–50°, and 50°–60°) to retrieve day-to-day variations under similar viewing angles. To further exclude seasonal variation, the angle-fixed series used in this research is only composed of observations in July, August, September, when the seasonal variation is relatively weak (see section 4.2). Variations in angle-fixed series are mainly day-to-day variations caused by actual daily artificial light change and daily changing environmental factors (e.g., atmospheric conditions and moonlight).

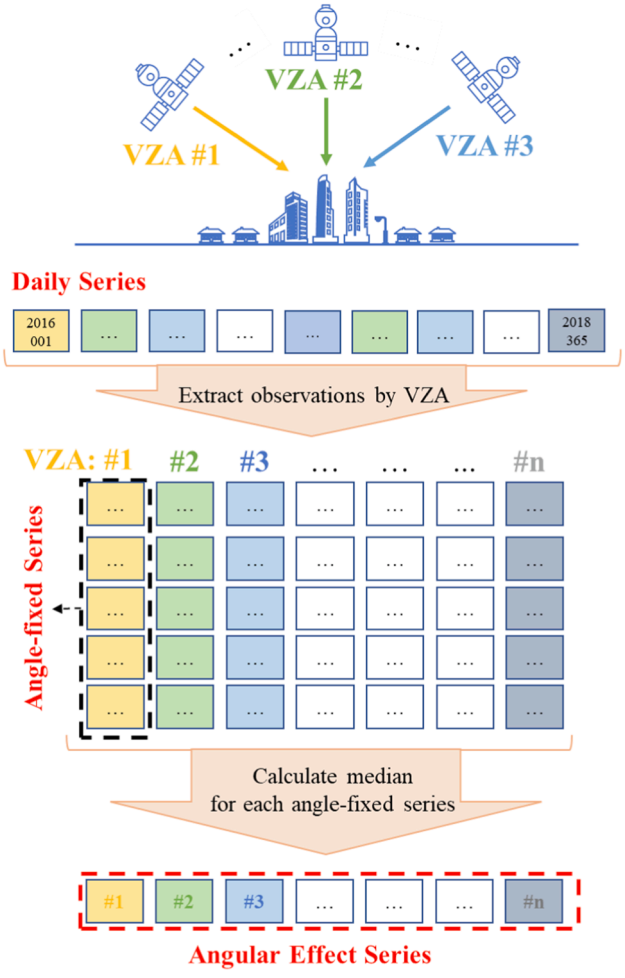


**Fig. 3.** Illustrative diagram of extracting angle-fixed and angular effect series from daily NTL series.

- **Angular effect series:** composed of median values of each angle-fixed series. Since the median value could exclude the observations under extreme conditions, it can represent the average situation of NTL observation at a certain angle. The variation in angular effect series mainly reflects the influence of satellite VZA. This study does not investigate the satellite azimuth angle separately due to its limited impact (Tan et al., 2022).

Variations in NTL were investigated on four spatial scales in the spatial–temporal hierarchical analysis module. First, variations were calculated from the abovementioned four grid-level temporal series. Subsequently, the grid-level temporal series or statistics were summarized to urban and regional scales to construct an overall picture of NTL variation. Finally, these statistics are also aggregated on different NTL brightness levels to understand NTL variation comprehensively, as the influence of various influential factors in brighter areas (e.g., urban centers) and darker areas (e.g., rural areas) may be different or even opposite.

Several metrics were used in this research to quantify the variation mentioned above, including standard deviation (SD) and coefficient of variation (CV):

$$CV = \frac{SD}{\overline{X}} \tag{1}$$

where $\overline{X}$ is the mean value, CV is a standardized measure of variability and can be used to compare the dispersion of datasets of varying magnitude. A higher CV indicates more temporal changes. Normalized Difference between Hotspot and Darkspot NTL radiance ($NDHD_{NTL}$) (Wang et al., 2021) is used to quantify the angular characteristics of NTL along with VZA:

$$NDHD_{NTL} = \frac{NTL_{hotspot} - NTL_{darkspot}}{NTL_{hotspot} + NTL_{darkspot}} \tag{2}$$

where The NTL radiance records in each grid are binned into seven categories based on the corresponding VZA values, with intervals of 10 degrees per bin; $NTL_{hotspot}$ refers to the bin with the highest radiance, while $NTL_{darkspot}$ represents the bin with the lowest radiance.

### 3.2. Quantifying impacts of environmental factors and observational conditions on NTL variation

Daily NTL change is a compound result of artificial light variation, multiple effects caused by environmental factors and observational conditions, and noises. As these changes are lumped together in the daily NTL time series, identification of artificial light changes becomes challenging. Three GLM models were developed to compare the proportions of these effects contributing to the daily NTL variations (Table 1). This comparison is facilitated by the coefficient of determination ($R^2$), a statistical measure in regression analysis that indicates the proportion of variance in the dependent variable explained by the independent variable.

Model 1(Eq. (3)) separates the NTL time series into trend components and seasonality components by incorporating a logistic, a linear, and two harmonic terms. The sigmoid function is utilized to represent NTL changes resulting from land cover changes, as prior research (Zheng

**Table 1**
Terms included in each of the three generalized linear models.

| Terms | Model 1 | Model 2 | Model 3 |
|---|---|---|---|
| Trend and seasonality | √ | √ | √ |
| Linear term of environmental factors and observational conditions | | √ | √ |
| Non-linear term and interactive term of environmental factors and observational conditions | | | √ |

et al., 2021) has demonstrated its effectiveness in quantifying various urban development and shrinking stages. The linear term captures the gradual NTL trend during the research period, reflecting the influence of socio-economic development or decline. The two harmonic terms are widely employed to capture intra-annual seasonality in NTL time series (Xie et al., 2019).

$$\ln(NTL) = \frac{a}{1+e^{bt+c}} + d + ft + \sum_{1}^{k}\left[g_k \sin\left(\frac{2\pi kt}{T}\right) + h_k \cos\left(\frac{2\pi kt}{T}\right)\right] + \varepsilon \tag{3}$$

where $\ln(NTL)$ represents the natural logarithm of the daily NTL measurements, $t$ denotes the $t$-th observation of the daily NTL time series. The logistic term includes three parameters: $a$ for magnitude of change, $b$ for change rate, and $c$ for timing of change. $e$ is the base of the natural logarithm, $d$ represents pre-change or post-change value, and $f$ is the slope of gradual annual change. The harmonic terms ($g_k$ and $h_k$) capture seasonal effects. $k$ is set to 2 to consider both annual and semi-annual variations. The period $T$ for harmonic terms is set to 365 days.

Model 2 (Eq. (4)) includes linear terms to account for the impact of environmental factors and observational conditions (Eq. (5)), while building upon the existing components in Model 1:

$$\ln(NTL) = \frac{a}{1+e^{bt+c}} + d + ft + \sum_{1}^{k}\left[g_k \sin\left(\frac{2\pi kt}{T}\right) + h_k \cos\left(\frac{2\pi kt}{T}\right)\right] + \beta U_i + \varepsilon \tag{4}$$

$$\beta U_i = \beta_1 AOD_i + \beta_2 Moon_i + \beta_3 VZA_i + \beta_4 time_i \tag{5}$$

Environmental factors involved in the model include *AOD*, and lunar irradiance (*Moon*), while observational conditions are satellite viewing angle (*VZA*) and overpass time (*time*). Parameters $\beta_1 \sim \beta_4$ represents effects of environmental factors and observational conditions that potentially linearly affecting $log(NTL_i)$.

Model 3 (Eq. (6)) further included quadratic function (Eq. (7)) and interact terms (Eq. (8)) to capture the potential non-linear impact of environmental factors and observational conditions.

$$\ln(NTL) = \frac{a}{1+e^{bt+c}} + d + ft + \sum_{1}^{k}\left[g_k \sin\left(\frac{2\pi kt}{T}\right) + h_k \cos\left(\frac{2\pi kt}{T}\right)\right] + \beta U_i + \gamma V_i + \delta W_i + \varepsilon \tag{6}$$

$$\gamma V_i = \gamma_1 AOD_i^2 + \gamma_2 Moon_i^2 + \gamma_4 VZA_i^2 + \gamma_5 time_i^2 \tag{7}$$

$$\delta W_i = \beta_1 VZA_i \times AOD_i + \beta_2 VZA_i \times Moon_i + \beta_3 AOD_i \times Moon_i \tag{8}$$

The above-mentioned models were constructed and estimated for each grid cell. The comparison between the three models is facilitated by the coefficient of determination ($R^2$), a statistical measure in regression analysis that indicates the proportion of variance in the dependent variable explained by the independent variable.

The average marginal effect (AME) of each explanatory variable is calculated to examine their overall impact on daily NTL, while accounting for the effects of other variables in the model. The spatial variability of explanatory variable effects can be revealed by establishing a generalized linear model and calculating the marginal effect for each pixel.

## 4. Results

### 4.1. Spatial-temporal patterns of daily NTL variation

The variation in four types of NTL series was visualized using a false-color composite of variation metrics (Fig. 4). The mean, standard deviation (*SD*), and coefficient of variation (*CV*) of the daily series are assigned to the red, green, and blue channels, respectively. The same color bar is used in the subplots of Fig. 4 to facilitate comparison. Background grid cells with an annual average NTL radiance<0.5 nW/cm$^2$/sr are discarded.

Significant differences between urban and rural areas were observed in the daily series of the NTL (Fig. 4 (a) and (b)). Cities are predominantly warm colors, indicating a high level of NTL brightness, a high *SD* value, but a low *CV* value. Rural areas are predominantly blue and dark, implying a low average NTL brightness with a high degree of variability (i.e., high *CV*). Daily NTL series variations exhibit distinct latitudinal patterns, particularly in urban areas. Above 40°N, urban areas are typically in a yellow-green tone, indicating high brightness and substantial fluctuations. Lower latitude cities are generally colored yellow-orange, indicating minor variation.

Fig. 4 (c) and (d) show the spatiotemporal pattern of seasonality, i.e., variation metrics are calculated using seasonal series derived from NTL data. The seasonality exhibits a latitudinal pattern similar to the daily series. Considering that the Collection V001 of Black Marble daily products still retains the seasonal effects of vegetation and snow, seasonality could be a significant contributor to the latitudinal patterns observed in the daily NTL variation. However, the color of cities is more towards red (i.e., lower *SD* than daily series), suggesting that seasonality may explain the variation on the daily scale to some extent. Fig. 4 (e) and 4 (f) exhibit the spatial pattern of angular effect, i.e., variations in angular effect series derived from the daily NTL dataset. The angular effect is mainly concentrated in urban areas, and no latitudinal pattern is observed. The angle-fixed series reflects the day-to-day NTL fluctuations, excluding angular and seasonal effects in the NTL dataset. As shown in Fig. 4 (g) and 4 (h), the angle-fixed series also shows urban–rural variability, i.e., higher *SD* and lower *CV* in cities, and higher *CV* in the suburbs. There is no clear latitudinal pattern in cities, but differences on a regional scale were observed in non-urban areas.

### 4.2. Comparison of different uncertainty sources

Jointly influenced by various factors, the variation in daily NTL time series is a combination of seasonality, angular effects, and deviation owing to daily changing factors. To compare and differentiate uncertainty from these sources, the standard deviation in daily (Fig. 5 (a)-(b)), seasonal (Fig. 5 (c)-(d)), angle-fixed (Fig. 5(e)-(f)), and angular effect series (Fig. 5 (g)-(h)) is measured on multiple NTL brightness levels. In daily series, *SD* is typically between 25% and 50% of the radiance, and the instability is stronger on darker grid cells. By comparison, the East Asia site exhibits less variation than the Northern America site.

Based on the standard deviation observed in the seasonal time series (Fig. 5 (c)-(d)), it can be inferred that seasonality constitutes a crucial contributor to the fluctuations observed in both study areas, although there exist notable variations between the two regions. Seasonality accounted for an SD of approximately 25% of the magnitude of NTL brightness in the North American site, with variations ranging from 10% to 50% (Fig. 5 (c)). By contrast, the average SD of NTL seasonality in the East Asia site is approximately 10% of NTL brightness, with minor differences which do not exceed 25% in most grid cells (Fig. 5 (d)). Variability of seasonality is also more pronounced in the suburbs than in urban centers. For example, grid cells with NTL radiance < 20 nW/cm$^2$/sr in the Northern America site may exhibit a seasonality of *SD* up to a comparable magnitude of its annual NTL radiance, while the ratio is approximately 50% in the East Asia site.

The ratio of monthly NTL radiance to that of June in urban areas is utilized to investigate the seasonality of each subregion and explore spatial differences in seasonality (Fig. 6). In Northern American cities above 40°N, the average NTL radiance in winter is approximately 1.5 times of summer, while the ratio is around 1.2 in cities at 30°N − 40°N. Vegetation and snow effects are the primary contributors to seasonal variation, as these effects remain uncorrected in the current version of the daily NTL product. However, cities in East Asia exhibited weaker seasonality at the same latitudes. Compared to previous research (Levin 2017) that investigated seasonality using monthly NTL

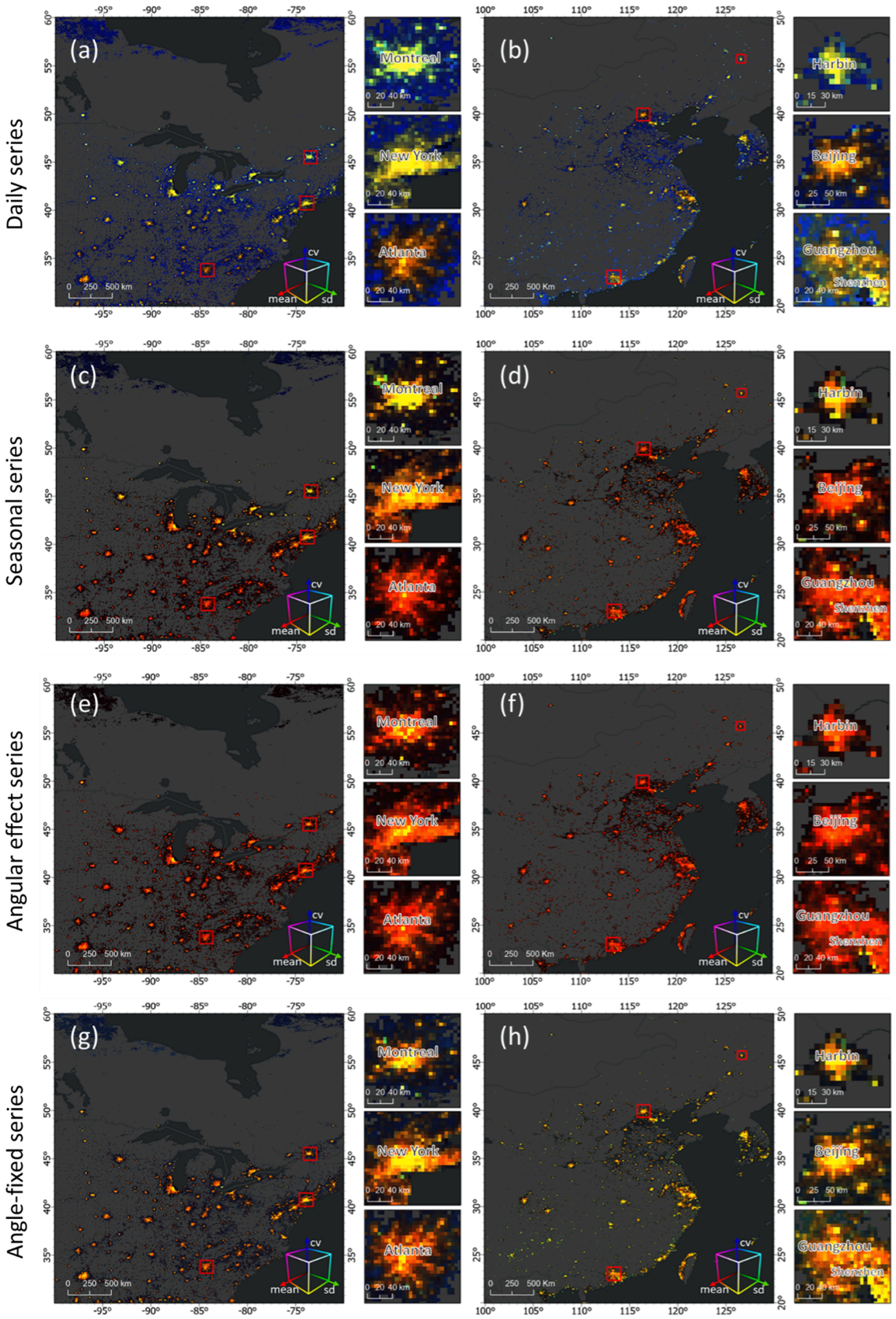


**Fig. 4.** Temporal variation in four types of NTL series in the two study areas. Maps are false-color composited by red, green and blue, representing the mean, standard deviation (*SD*), and coefficient of variation (*CV*) of each NTL series. (For interpretation of the references to color in this figure legend, the reader is referred to the web version of this article.)

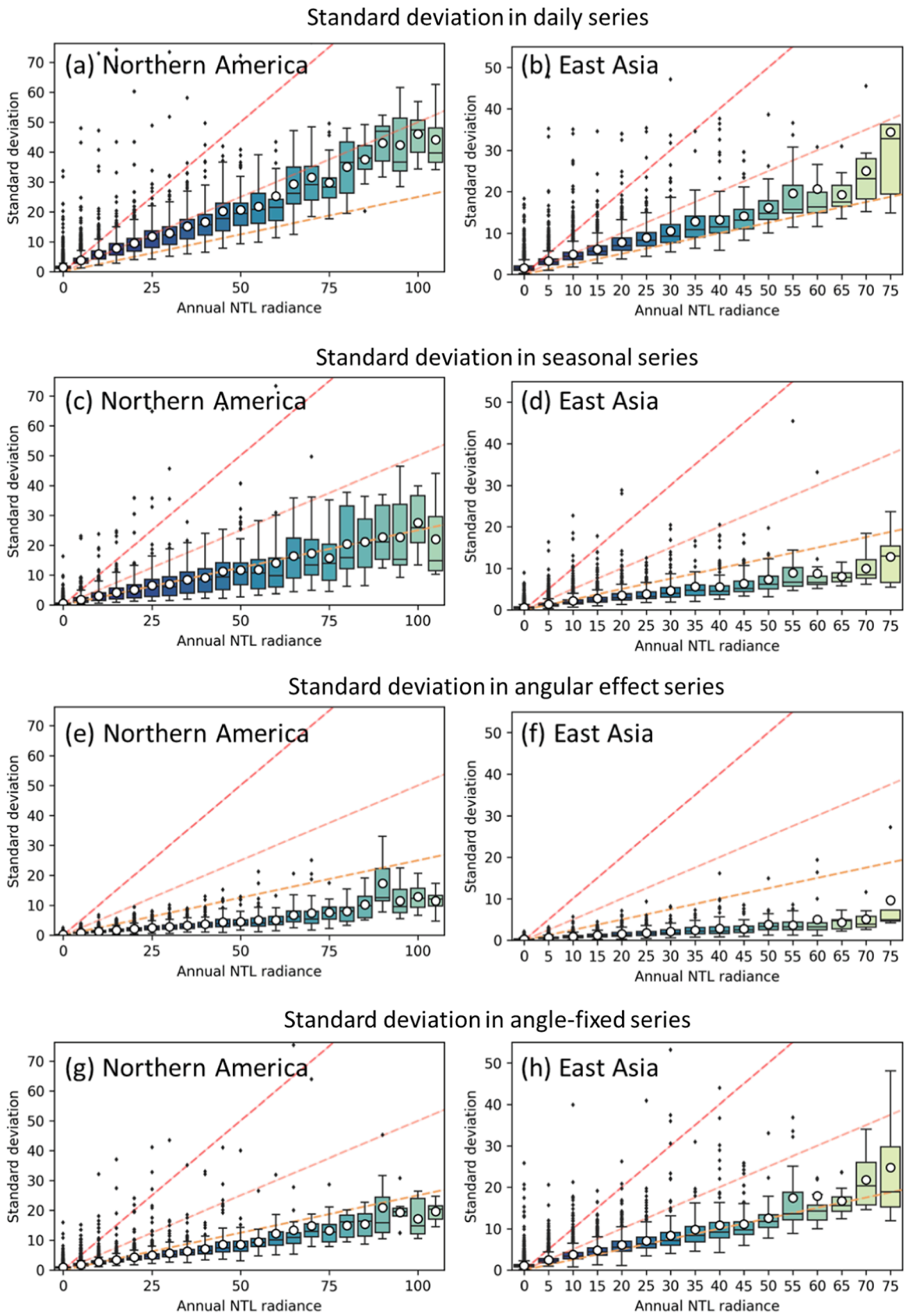


**Fig. 5.** Boxplots of the *SD* of daily series (a-b), seasonal series (c-d), angular effect series (e-f), and angle-fixed series (g-h) of at different NTL brightness in Northern America and East Asia. The box shows the quartiles and median, the whiskers extend to show range while the dots outside show outliers. Mean values are displayed with a white dot. From top to bottom, the three dotted lines representing x:y = 1:1, x:y = 1:0.5, and x:y = 1:0.25, respectively.

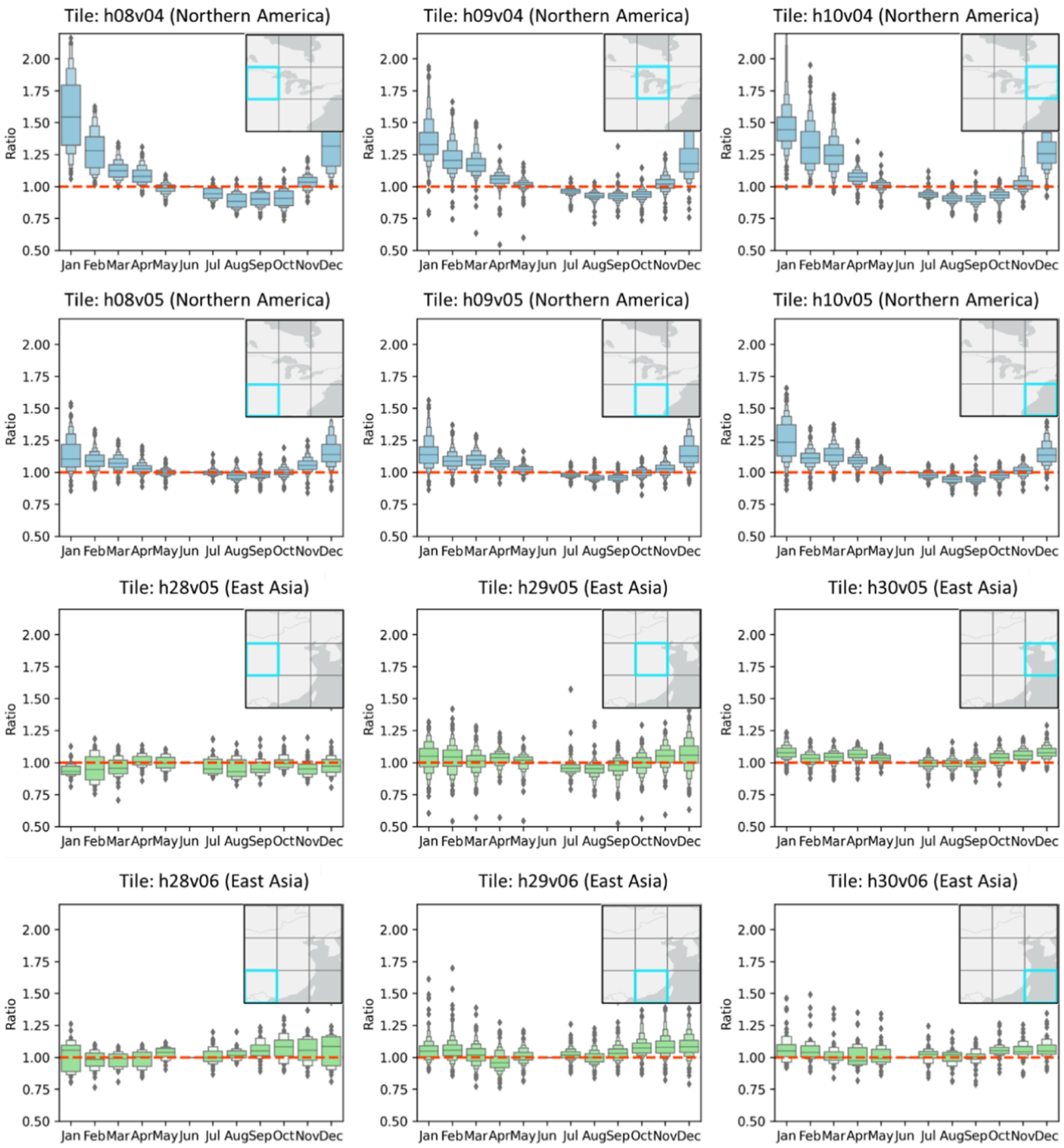


**Fig. 6.** Boxplots of the ratio of monthly NTL radiance to that of June in urban areas of Black Marble tiles in the study areas (refer to highlighted tile in the thumbnail map on the upper right corner). The box shows the quartiles and median of the NTL relative ratio; the whiskers extend to show range while the diamonds outside show outliers.

composites without moonlight and atmospheric correction, this experiment reveals similar latitudinal patterns but with weaker seasonality.

To comprehensively explore the spatial variability of angular effects, the NDHD is calculated at the grid, urban, and brightness levels of NTL. As shown in Fig. 7 (a) and (b), at the urban scale, stronger angular effects are generally observed in Northern American cities compared to those in East Asian cities. Fig. 7(c) and (d) illustrate the statistics of NDHD at the grid scale within these cities. The median NDHD in over two-thirds of Northern American cities exceeds 0.1, while such levels of angular effect intensity are only observed in a few East Asian cities. The angular effect originated from varying emitted power and radiance of NTL with angle due to the urban street layout, location of the light source, and building height (Li et al., 2022; Tan et al., 2022). Northern American cities are typically characterized by dense high-rise commercial centers and extensive homogeneous low-rise buildings, both of which contribute to a strong angular effect. In contrast, East Asian cities have taller buildings but with less density, resulting in a weaker angular effect.

Fig. 7(e) and (f) illustrate how the NTL radiance varies with the viewing angle. For each brightness level, the NTL variation of Northern American grid cells is more drastic than that of East Asian cities. An average of 1.25 times brighter NTL radiance than nadir was observed at VZA of over 60° in Northern America grid cells, while the ratio is 1.02 in

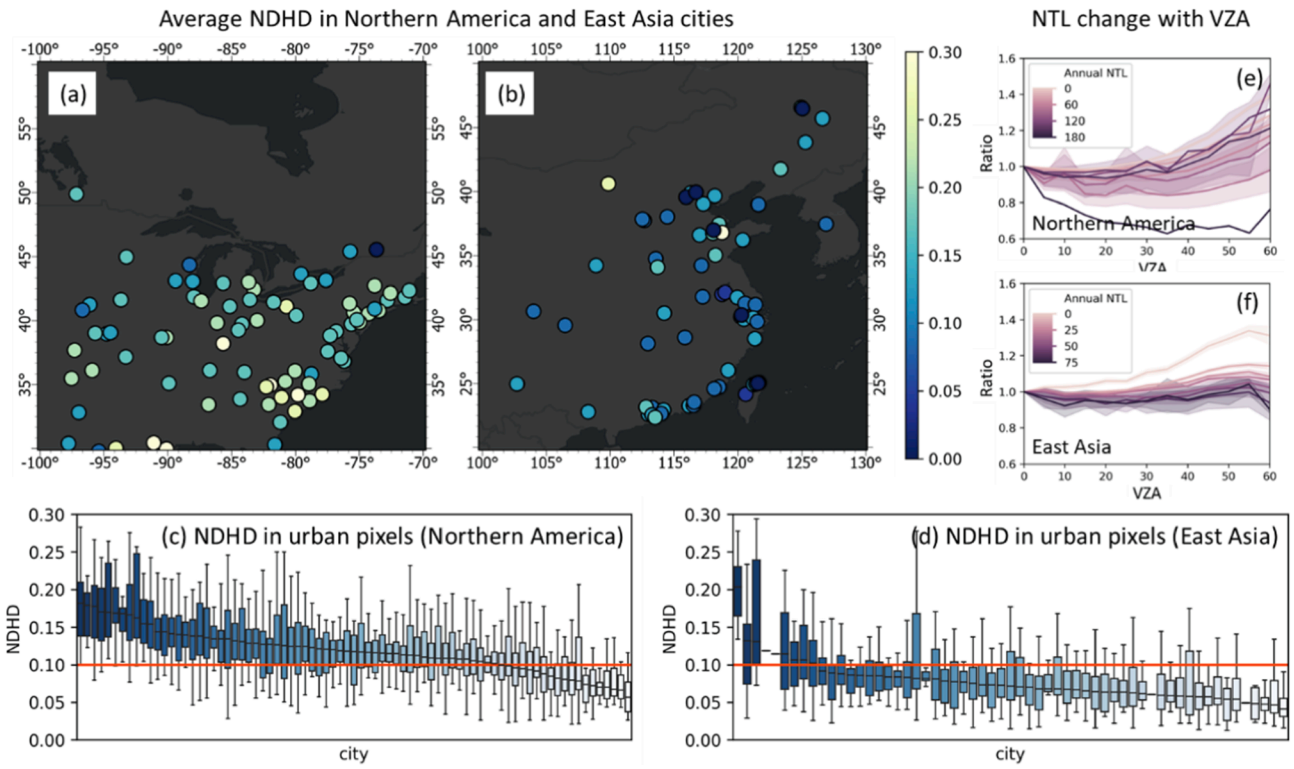


**Fig. 7.** Average NDHD at the city level in Northern America (a) and East Asia (b). Boxplots show statistics of NDHD at the grid level in each city in Northern America (c) and East Asia (d). NTL radiance change ratio at different angles to that of nadir in Northern America (e) and East Asia (f).

East Asia grid cells. Specifically, in highly illuminated urban areas of North America, a decrease in light intensity with observation angle can be observed, whereas it is not as prominent in East Asian cities.

### 4.3. Contribution of environmental factors and observational conditions

The results obtained from an urban and a rural grid cell are illustrated in Fig. 8 as examples of good-of-fitness of the three models, revealing that Model 3 exhibits superior performance. It is understandable that due to human activities being a major contributor to NTL change, the proposed models cannot achieve a perfect fit. Nevertheless, the goodness-of-fit of the models facilitates the identification of the portion of NTL change attributable to environmental factors and observational conditions.

The statistics of R-squared for the three models across the two regions are presented in Fig. 9. In general, seasonal effects only account for a limited portion of variation in daily NTL time series, with the 25th and 75th percentiles across all grids in the two research regions being 3.42% and 13.63%, respectively. Thses values indicating that seasonality is overshadowed by day-to-day changes when modeling daily NTL variations. However, by considering environmental factors and observational conditions, a larger portion of daily variations can be explained, ranging from 17.17% to 35.25% for the 25th and 75th percentiles. Furthermore, the inclusion of non-linear and interactive effects in the model contributes to even more explained variations, with percentages ranging from 25.41% to 44.89% for the 25th and 75th percentiles.

Based on the comparison, Model 3 was utilized to assess the impact of environmental factors and observational conditions. To ensure the credibility of the results, only models and marginal effects that passed the T-test (p-value $< 0.05$) were considered in subsequent analyses. Fig. 10 shows the $R^2$ values of the models established for each grid. The models were significant for 98.60% of the Northern American grid cells and 94.88% of the East Asian grid cells, including 97.39% of the Northern American urban grid cells and 91.15% of the East Asian urban grid cells. Sub-regions A-J demonstrate the spatial variations of model fitting in urban and suburban areas. As the coefficient of determination in cities is generally lower than in rural areas, it can be inferred that environmental and observational condition factors account for a larger proportion of daily NTL change in rural areas than in cities, while NTL change in cities is more influenced by human activities. This observation is likely due to the fact that daily NTL changes in urban areas are more susceptible to influences from human activities, such as traffic patterns, social events, and temporal lightings (Liu et al., 2022). In contrast, suburban areas are less impacted by such human-related factors (Gao et al., 2023), allowing the environmental and observational condition variables to exert a more significant influence on the daily NTL variations.

Fig. 11 (a) and (b) present the marginal effects of AOD based on NTL radiance levels. The results indicate that 39.19% of North American pixels and 30.49% of East Asian pixels are significantly affected by AOD (p-value $< 0.05$ in Model 3). The impact of AOD exhibits a distinct rural–urban spatial pattern, as shown in the magnified subregion in Fig. 11 (c). The marginal effects inside and outside the urban boundary show opposite tendencies. In urban areas, the NTL radiance is typically weakened by aerosols, whereas in suburban areas, the weakening effect is less prominent, and often, an increase in AOD leads to an augmentation in observed light intensity. Specifically, for the low-light grid cells (i.e., with NTL radiance$<10$ nW/cm$^2$/sr), an increase of 0.1 AOD can cause an average increase of daily NTL radiance by 2.25% in Northern America. On the contrary, for the grid with light radiance greater than 10 nW/cm$^2$/sr, the effect of aerosols is mostly negative, and an increase of 0.1 AOD can cause an average decrease of NTL observations by 4.32% and 1.33% in Northern America and East Asia, respectively. Despite the difference in the magnitude of AOD impact between the two regions, the spatial pattern of rural–urban difference is similar.

Fig. 12 (a) and (b) present statistical results of the marginal effects of moonlight based on NTL radiance levels. In general, significant marginal effects (p-value $< 0.05$) of moonlight were detected in 55.78% of grid

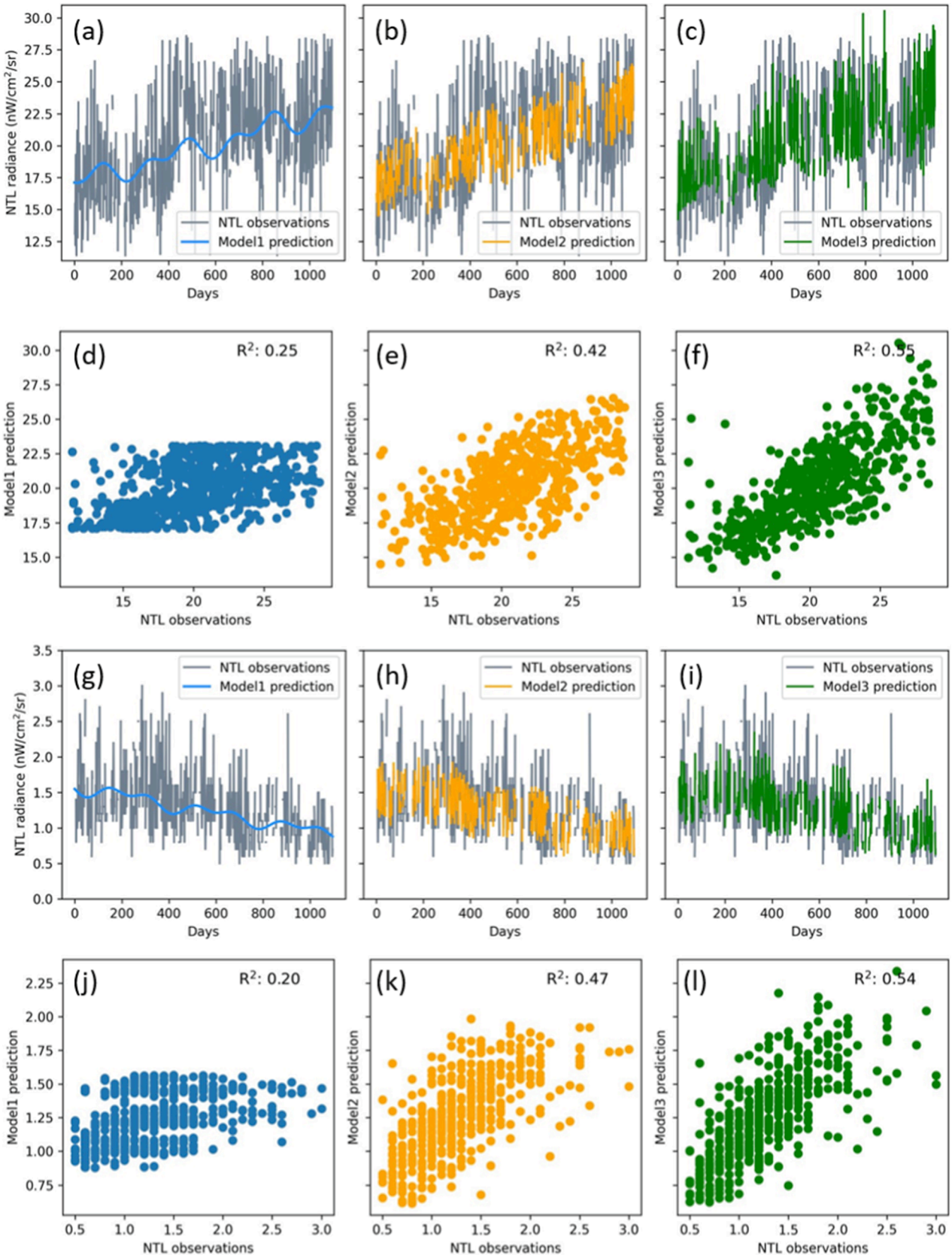


**Fig. 8.** Original NTL time series and predicted time series by Model 1 ~ 3 in an urban sample (a ~ c), and scatter plot between the NTL observations and predictions (d-f). Original NTL time series and predicted time series by Model 1 ~ 3 in an rural sample (g ~ i), and scatter plot between the NTL observations and predictions (j-l).

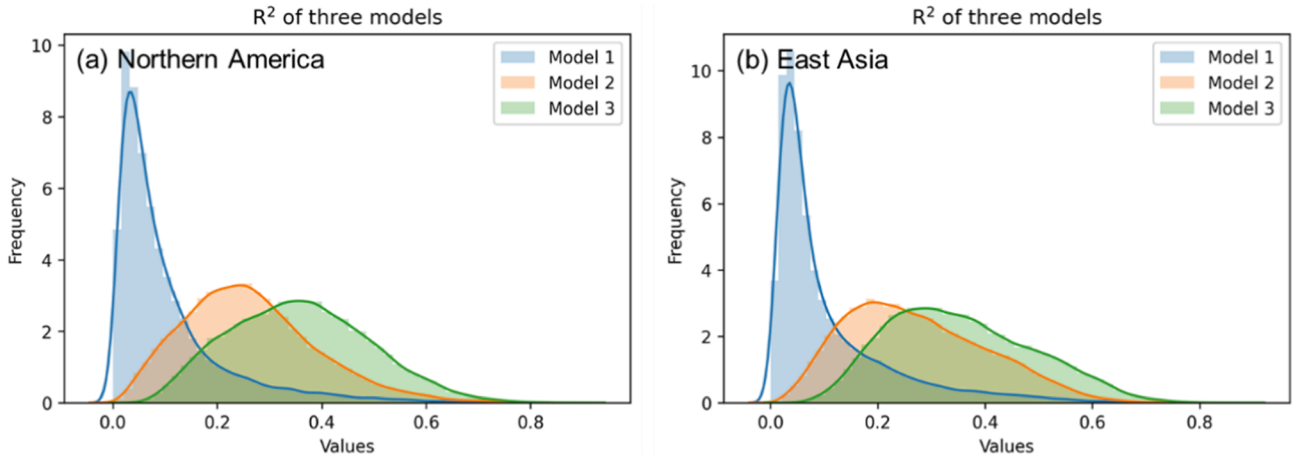


**Fig. 9.** The histogram of R-squared values for the three proposed models across (a) Northern America and (b) East Asia.

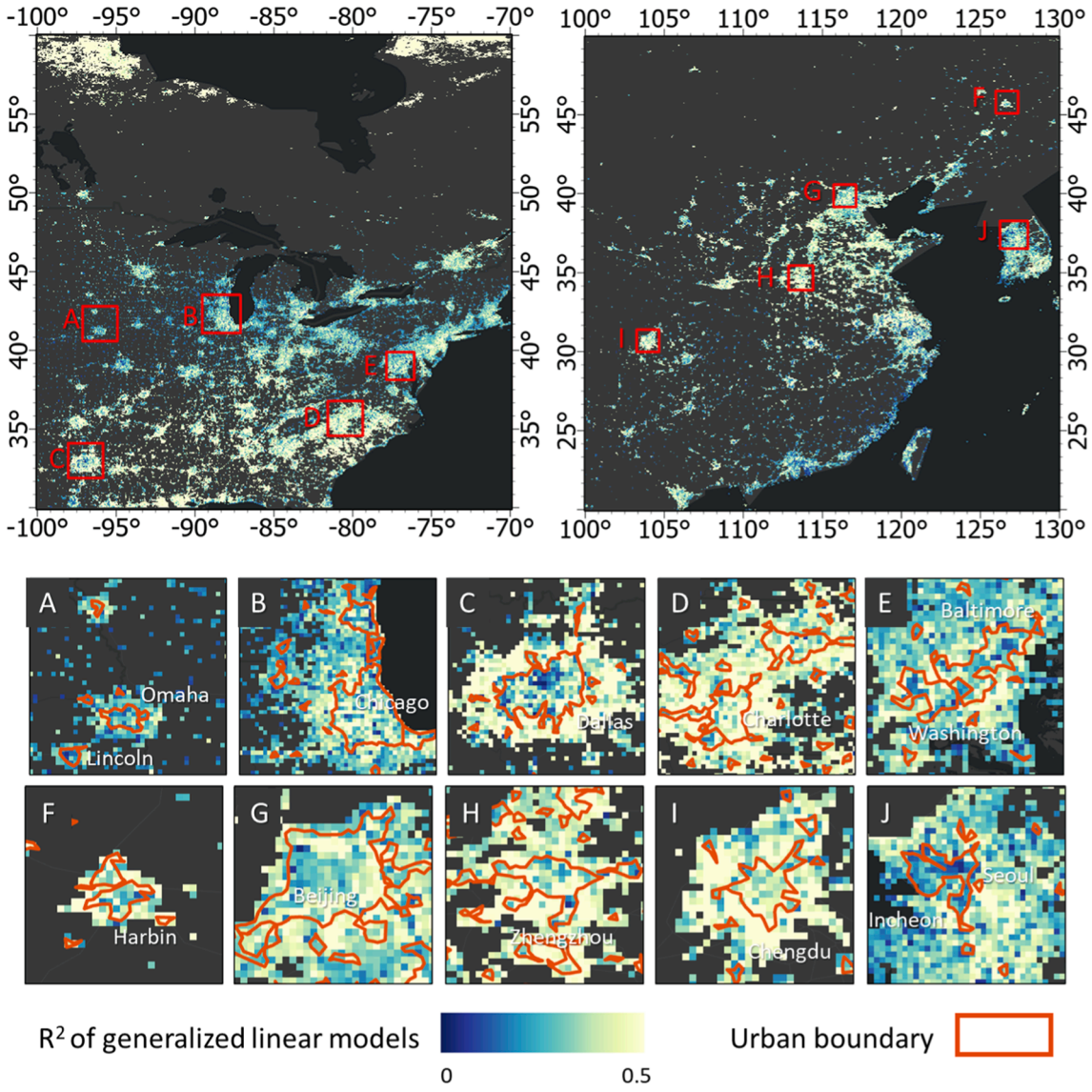


**Fig. 10.** $R^2$ of Model 3 in Northern America and East Asia. The red boxes indicate the extent of ten selected sub-regions, and the orange boundary depicts the urban extent obtained from impervious surface products. (For interpretation of the references to color in this figure legend, the reader is referred to the web version of this article.)

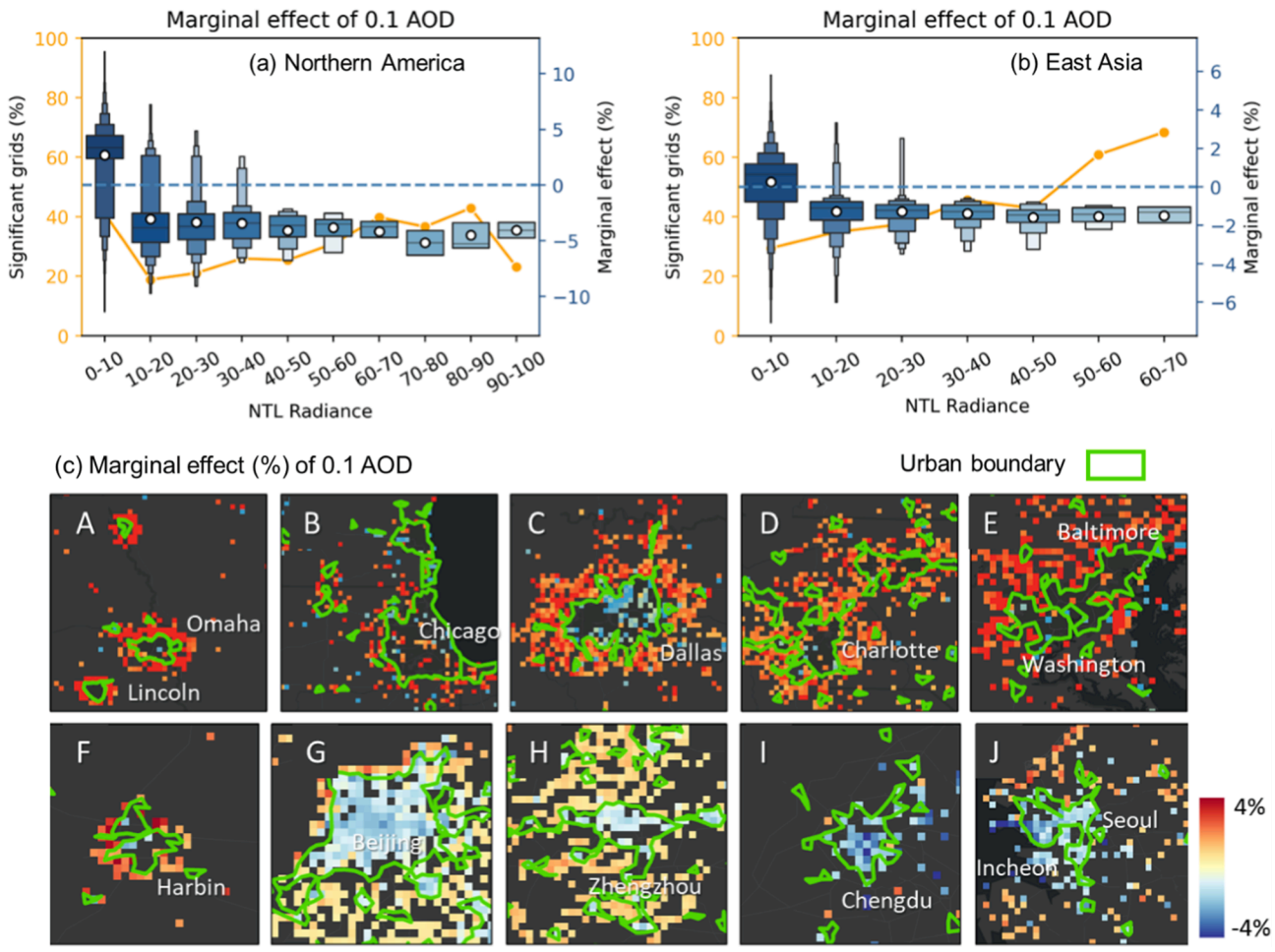


**Fig. 11.** Boxplots depict the statistical results of the marginal effects of AOD derived from Model 3 in Northern America (a) and East Asia (b) grouped by NTL radiance level. The yellow lines show the proportion of grid cells in each group that exhibit significant marginal effects (p-value < 0.05); The zoomed-in maps (c) display the marginal effects of AOD in ten sub-regions, with the location and extent of the sub-regions marked in Fig. 10, and the urban boundary obtained from impervious surface products shown in green. (For interpretation of the references to color in this figure legend, the reader is referred to the web version of this article.)

cells in North American sites and 41.28% of grid cells in East Asian sites, with most of these grid cells located in low-light areas outside urban boundaries (as shown in Fig. 12(c)). In grid cells with annual NTL radiance below 10 nW/cm$^2$/sr, moonlight showed significant effects (p-value < 0.05) on 60.00% of North American pixels and 44.80% of East Asian pixels, while the proportion of significant moonlight effects (p-value < 0.05) rapidly declined in areas with higher ground light radiance.

According to previous research (Wang et al., 2021), moonlight would boost satellite-observed radiance with a magnitude comparable to artificial light radiance in rural and suburban areas. The statistical results of this experiment indicate that the impact of moonlight has been greatly attenuated in terms of the strength of marginal effects during the Black Marble correction. However, it is worth noting that negative marginal effects of moonlight were detected, indicating that in some areas (mainly concentrated in suburbs (Fig. 12(c)), the effect of moonlight may have been overestimated in the correction process. Take the 25% and 75% quantile of all significant (p-value < 0.05) grid cells as example, whoes margial effect of them are 0.056% and −0.116%, respectively. This implies that a full moon, with approximately 140 nW/cm$^2$ lunar irradiance, would lead to an 8.15% increase and a 14.99% decrease in NTL observations, respectively.

As shown in Fig. 13 (a)-(b), the influence of VZA is widely present in the corrected daily NTL, with 96.26% of Northern American grid cells and 87.43% of East Asia grid cells being affected. The marginal effect of VZA shows a clear urban–rural gradient. For example, for grid cells with annual NTL radiance<10 nW/cm$^2$/sr, a 1-degree increase in VZA can cause an average increase of 0.52% in daily NTL radiance for Northern American grid cells and 0.46% for East Asian grid cells. In brighter grid cells, such as those in the group of 50–60 nW/cm$^2$/sr, the average marginal effect of VZA decreases to 0.33% and 0.06% for Northern America and East Asia, respectively. In the brightest areas of urban regions, negative marginal effects of VZA were observed. Furthermore, there are notable differences in the impact of VZA between the two study sites in Northern America and East Asia. First, the angular effect is more prevalent within urban areas of the Northern America site, where there are more urban grid cells with significant marginal effects of VZA (p-value < 0.05). The disparities between them are more pronounced, particularly in densely populated areas with brighter illumination. Secondly, the occurrence of negative effects of VZA in the brightest areas of urban lights is more prevalent in the Northern America grid cells, whereas in the East Asia pixels, such negative effects are comparatively less widespread.

## 5. Discussion

### 5.1. Possible reasons for the remaining variations in Black Marble product

This study aims to examine the influence of environmental and observational factors on the corrected daily NTL, given that some factors

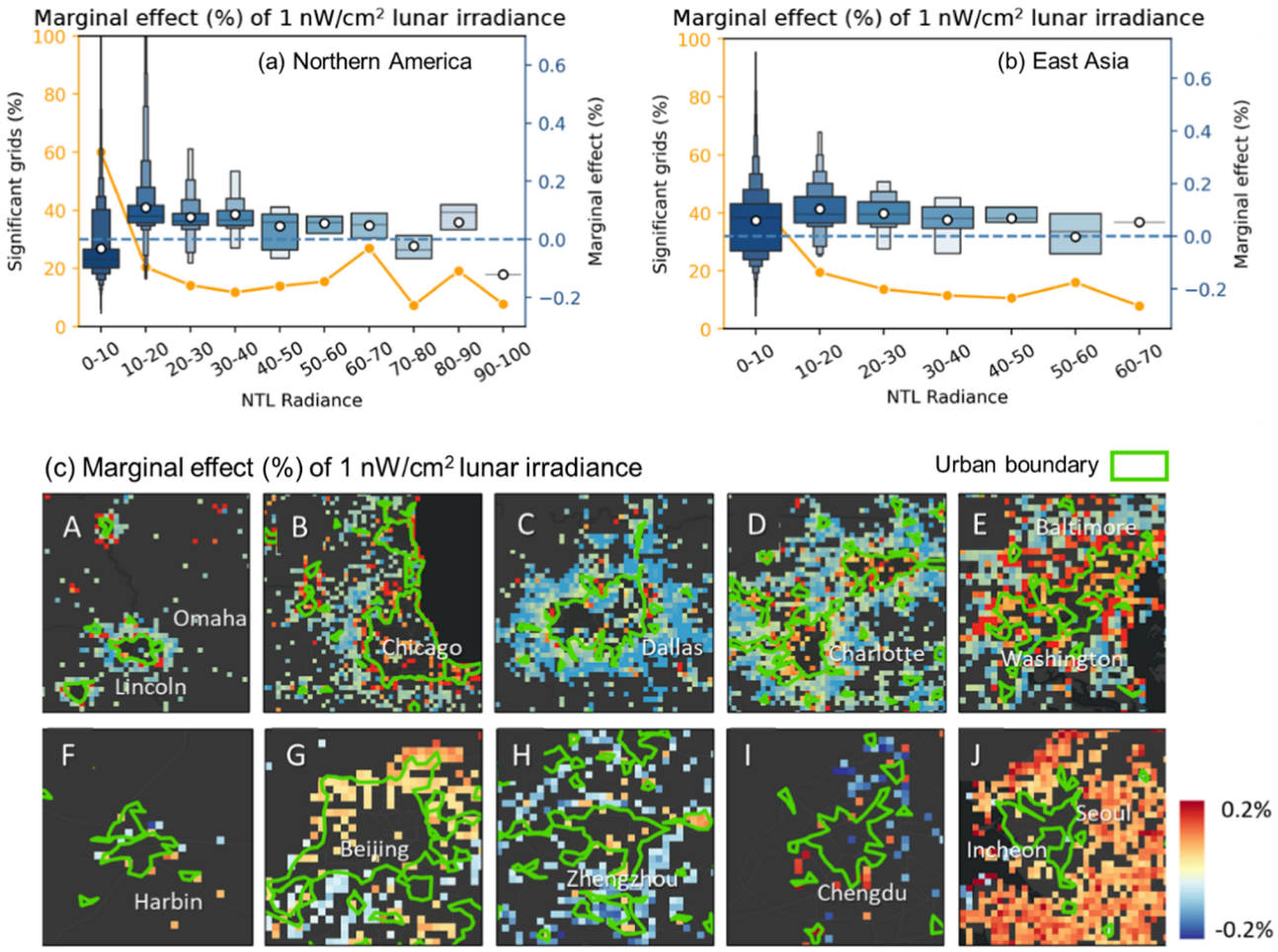


**Fig. 12.** Boxplots depict the statistical results of the marginal effects of lunar irradiance derived from Model3 in Northern America (a) and East Asia (b) grouped by NTL radiance level. The yellow lines show the proportion of grid cells in each group that exhibit significant marginal effects (p-value < 0.05); The zoomed-in maps (c) display the marginal effects of lunar irradiance in ten sub-regions, with the location and extent of the sub-regions marked in Fig. 10, and the urban boundary obtained from impervious surface products shown in green. (For interpretation of the references to color in this figure legend, the reader is referred to the web version of this article.)

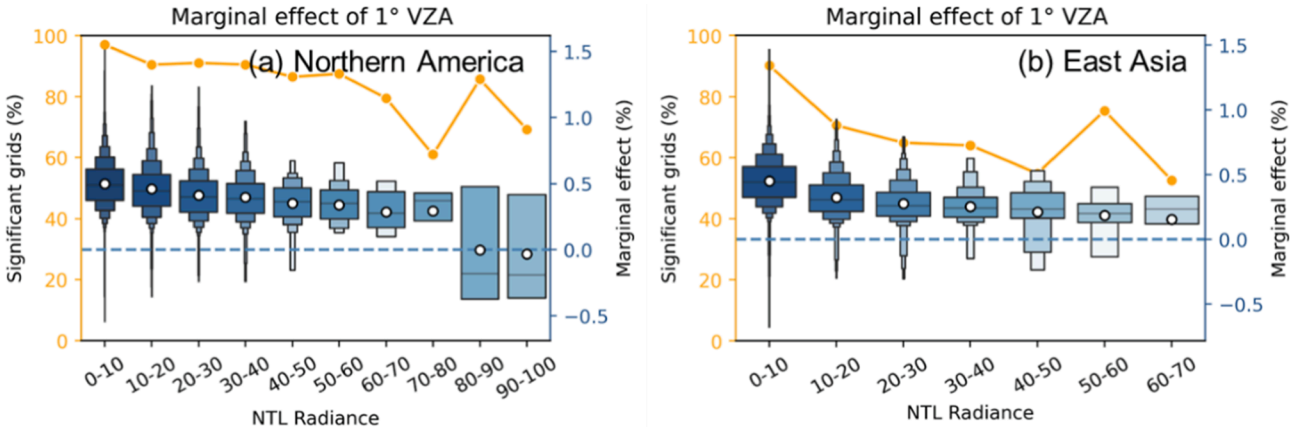


**Fig. 13.** Boxplots depict the statistical results of the marginal effects of VZA derived from Model 3 in Northern America (a) and East Asia (b) grouped by NTL radiance level.

may have their impact weakened or modified post the lunar BRDF correction. For example, the impact of AOD exhibited spatial patterns (Fig. 11), which differ from conclusions drawn on TOA radiance data in a previous study (Wang et al., 2021). It is because the environmental impacts concluded in this research are based on the corrected daily NTL series, thus the results reflect impacts that persist after correction. A potential reason for the positive impact of AOD in low-light areas is that aerosols scatter light downward, thus contributing to the blooming effect in the outskirts (Cao et al., 2019).

The impact of moonlight on satellite-observed NTL has been

substantially corrected in the Black Marble product suite, but significant marginal effects of moonlight (p-value $< 0.05$) were found in both research regions. Potential sources of the impact include: First, reflected lunar radiance is corrected with surface BRDF/albedo, and lunar irradiance is calculated based on the radiometry-based lunar irradiance model (MT2009), containing uncertainty on the order of 7–12% (Miller and Turner, 2009). Second, reflected lunar radiance also rises with higher albedo. However, albedo data from MCD43/VNP43 products have been retrieved with relatively lower quality in some regions, such as Southern China and high northern latitudes (Liu et al., 2017). The spatial pattern of lunar effect in Fig. 12 may be explained by these uncertainties and other higher-order effects omitted in the NTL radiance correction procedure.

### 5.2. Innovations and insights

This research proposed a novel framework that effectively separates the influences of multiple factors on daily NTL time series, leading to a comprehensive understanding of corresponding uncertainties. By employing different slicing and composition techniques, four distinct types of NTL series were generated, with each series being dominated by specific factors that contribute to the variations in NTL. This approach enables the separation and comparison of uncertainties within daily NTL time series. In contrast to previous studies that focused on selected sites and specific time periods to evaluate the impact of individual factors, our proposed strategy allows for comprehensive evaluations and comparisons of spatiotemporal patterns of uncertainty in larger regions. Furthermore, future studies can adopt this framework to explore variations and driving factors at different spatial and temporal scales, as well as consider other sources of daily NTL data.

This research has made significant contributions by evaluating uncertainties in daily NTL time series across various spatial and temporal scales, leading to essential insights for the future utilization of such data. First, this research enhanced understanding of the impact of environmental and observational factors on daily nighttime light data, contributing valuable insights for studying ground artificial light dynamics. In general, seasonal effects contribute only to a limited portion of NTL variation. With the consideration of environmental factors and observational conditions, approximately 25%~50% of the daily variations can be explained. The remaining half or more of the variation is primarily influenced by real artificial light changes and other noises.

Secondly, this research offers valuable insights into future works on removing the daily NTL uncertainty. By understanding the impacts of different types of variations, users can make informed decisions regarding the most efficient approach to preprocess the daily NTL time series. For instance, in Northern America, where seasonal variation is more pronounced, it is crucial to decompose seasonality before conducting further analysis. Conversely, in East Asia, where seasonality is less pronounced, greater attention should be directed towards day-to-day changing factors, as they have a more significant influence on daily NTL variations. Eliminating impact of angualr effect (Jia et al., 2023) can ensure more accurate and reliable comparisons of NTL between individual days.

Thirdly, this research places emphasis on the spatial heterogeneity of uncertainties in daily satellite nighttime light time series, which can guild the future studies in different regions. In contrast to previous studies that primarily focused on the influence of specific environmental or observational factors in selected cities, our research conducted a comprehensive exploration of the spatial variability of these impacts across larger regions. This provides essential background knowledge when analyzing NTL changes detected from NTL time series. For example, the angular effect is usually more pronounced in cities in Northern America than in cities in East Asia, due to differences in urban structure and building characteristics. Impact of aerosols may vary between cities and rural areas. Hence, it is appropriate to consider the effects of different environmental factors accordingly when interpreting daily NTL data across various locations.

Finally, this research employed lunar-BRDF corrected daily NTL data, which represents the most advanced and promising product with broad applications. While previous studies have demonstrated the influence of environmental factors on TOA nighttime radiance or monthly composited datasets (Levin, 2017; Yuan et al., 2022), it is crucial to recognize that these impacts may attenuated or altered after the correction process. For instance, our findings indicate that significant lunar effects persist in some rural areas, while the impacts of aerosol and VZA exhibit variations correlated with surface NTL brightness.

### 5.3. Implications and future studies

This study is beneficial for future daily NTL studies. Uncertainty of NTL data on various temporal and spatial scales is essential for further processing or utilizing the variation of daily NTL datasets. Daily NTL time series are highly variable, so users should exercise caution when identifying changes or trends in artificial light from it. The variation of daily NTL varied greatly across locations. Thus, regional criteria for evaluating light changes should be established according to specific objectives in the applications. Black Marble corrected NTL dataset is recommended in applications to minimize the impact of environmental factors. However, in many cases, environmental factors still have a significant impact and should not be ignored. We hope that this research can provide insights for improving the correction strategies of daily NTL products.

In future research, the evaluation of daily NTL can be improved in the following aspects. First, the indicators used in this study cannot accurately characterize all environmental conditions. For example, some environmental factors are not considered because of data availability, such as tropospheric water vapor (Small, 2019) and near-surface pollutant concentrations. Daytime AOD is utilized in establishing the models as no nighttime AOD product is currently available. Although the difference between daytime and nighttime AOD is mostly$<0.1$ (Wang et al., 2021), in some locations, particularly in big cities, higher AOD differences are observed, leading to increased uncertainties in the modeling process. Second, misclassification errors in nighttime cloud masks may affect the assessment results. Third, this evaluation is conducted based on NASA's Black Marble product. The spatiotemporal patterns of NTL variation derived from other nighttime datasets may be different due to the inconsistency in data processing and correction procedures. In addition to the abovementioned environmental factors, the mechanism of daily NTL variation may involve more aspects, especially anthropogenic factors (Elvidge et al., 2022, 2020a; Román and Stokes, 2015). Thus further studies are needed to explore the mechanism of daily NTL fluctuation in cities.

## 6. Conclusion

This research explored the variation of the lunar BRDF-corrected daily NTL time series across various spatial–temporal scales and the impact of environmental factors. This research proposed a spatial–temporal hierarchical analysis strategy to separate the effects of multiple factors on daily NTL time series and evaluated variations from different sources. Generally, the standard deviation of the daily NTL time series is mostly around 25%-50% of the NTL radiance value. The daily NTL in Northern America has variations up to 50% of the annual average, which is stronger than in East Asia, with variations up to 25%. By separating uncertainties caused by different sources, we found that the intensity of uncertainties differs in the two regions. The variation in seasonality is stronger in Northern America, whereas the variation related to day-to-day changing factors is stronger in East Asia.

Furthermore, generalized linear models are built to capture the relationship between daily NTL and influential factors in each grid. The results show that approximately 25%~50% of the daily variations can be explained by environmental factors, observational factors and

seasonality. The remaining half or more of the daily variation is primarily influenced by real artificial light changes and noise. The influence of environmental and observational factors that vary on a daily basis should not be disregarded in the daily corrected NTL dataset as they form spatially heterogeneous changes in NTL radiance. For instance, an increase in AOD typically results in an augmentation of NTL in low-light rural regions, whereas a tendency towards a decline in NTL is observed in urban areas; The impact of moonlight is mainly concentrated in rural and low-light areas, whereas the lunar effect on daily NTL radiance in urban areas is minimal. Therefore, users are recommended to consider the influence of environmental factors accordingly when interpreting daily NTL at various scale levels and regions. This research revealed essential knowledge about variation of NTL and spatial pattern of environmental impact on the daily lunar-BRDF corrected NTL radiance, thus benefiting further utilizing and interpreting daily NTL datasets.

## CRediT authorship contribution statement

**Xiaoyue Tan:** Methodology, Software, Formal analysis, Investigation, Writing – original draft, Visualization. **Ruilin Chen:** Methodology, Investigation. **Xiaolin Zhu:** Conceptualization, Methodology, Resources, Writing – review & editing, Project administration, Supervision, Funding acquisition. **Xi Li:** Writing – review & editing, Funding acquisition. **Jin Chen:** Conceptualization, Methodology, Writing – review & editing. **Man Sing Wong:** Writing – review & editing, Funding acquisition. **Shuai Xu:** Writing – review & editing. **Yi Nam Xu:** Writing – review & editing.

## Declaration of Competing Interest

The authors declare that they have no known competing financial interests or personal relationships that could have appeared to influence the work reported in this paper.

## Data availability

The authors do not have permission to share data.

## Acknowledgements

This study was supported by the Research Grants Council of Hong Kong (project No.15229222), the National Natural Science Foundation of China (No. 42271371), and Guangdong Basic and Applied Basic Research Foundation (No. 2022B1515130001), and The Hong Kong Polytechnic University (project Nos. 4-ZZND and Q- CDBP). Man Sing Wong would like to thank the funding support (1-CD81) from the Research Institute for Land and Space, The Hong Kong Polytechnic University, Hong Kong, China. The authors would like to thank Dr. Luoma Wan for his constructive comments on the manuscript.

## References

Bennett, M.M., Smith, L.C., 2017. Advances in using multitemporal night-time lights satellite imagery to detect, estimate, and monitor socioeconomic dynamics. Remote Sens. Environ. 192, 176–197. https://doi.org/10.1016/j.rse.2017.01.005.

Cao, C., Shao, X., Uprety, S., 2013. Detecting light outages after severe storms using the S-NPP/VIIRS day/night band radiances. IEEE Geosci. Remote Sens. Lett. 10, 1582–1586. https://doi.org/10.1109/LGRS.2013.2262258.

Cao, X., Hu, Y., Zhu, X., Shi, F., Zhuo, L., Chen, J., 2019. A simple self-adjusting model for correcting the blooming effects in DMSP-OLS nighttime light images. Remote Sensing of Environment 224, 401–411. https://doi.org/10.1016/j.rse.2019.02.019.

Elvidge, C.D., Baugh, K.E., Kihn, E.A., Kroehl, H.W., Davis, E.R., 1997. Mapping city lights with nighttime data from the DMSP Operational Linescan System. Photogramm. Eng. Remote Sens. 63, 727–734.

Elvidge, C.D., Baugh, K., Zhizhin, M., Hsu, F.C., Ghosh, T., 2017. VIIRS night-time lights. Int. J. Remote Sens. 38, 5860–5879. https://doi.org/10.1080/01431161.2017.1342050.

Elvidge, C.D., Ghosh, T., Hsu, F.C., Zhizhin, M., Bazilian, M., 2020a. The dimming of lights in China during the COVID-19 pandemic. Remote Sens. 12, 2851. https://doi.org/10.3390/RS12172851.

Elvidge, C.D., Hsu, F.-C., Zhizhin, M., Ghosh, T., Taneja, J., Bazilian, M., 2020b. Indicators of Electric Power Instability from Satellite Observed Nighttime Lights. Remote Sens. 12, 3194. https://doi.org/10.3390/rs12193194.

Elvidge, C.D., Zhizhin, M., Keith, D., Miller, S.D., Hsu, F.C., Ghosh, T., Anderson, S.J., Monrad, C.K., Bazilian, M., Taneja, J., Sutton, P.C., Barentine, J., Kowalik, W.S., Kyba, C.C.M., Pack, D.W., Hammerling, D., 2022. The VIIRS Day/Night Band: A Flicker Meter in Space? Remote Sens. 14, 1316. https://doi.org/10.3390/rs14061316.

Gao, P., Wu, T., Ge, Y., Yang, G., Lu, Y., 2023. Correcting the nighttime lighting data underestimation effect based on light source detection and luminance reconstruction. Int. J. Appl. Earth Obs. Geoinformation 121, 103380. https://doi.org/10.1016/j.jag.2023.103380.

Guo, B., Hu, D., Zheng, Q., 2023. Potentiality of SDGSAT-1 glimmer imagery to investigate the spatial variability in nighttime lights. Int. J. Appl. Earth Obs. Geoinformation 119, 103313. https://doi.org/10.1016/j.jag.2023.103313.

Huang, Y., Song, Z., Yang, H., Yu, B., Liu, H., Che, T., Chen, J., Wu, J., Shu, S., Peng, X., Zheng, Z., Xu, J., 2022. Snow cover detection in mid-latitude mountainous and polar regions using nighttime light data. Remote Sens. Environ. 268, 112766 https://doi.org/10.1016/j.rse.2021.112766.

Jia, M., Li, X., Gong, Y., Belabbes, S., Dell'Oro, L., 2023. Estimating natural disaster loss using improved daily night-time light data. Int. J. Appl. Earth Obs. Geoinformation 120, 103359. https://doi.org/10.1016/j.jag.2023.103359.

Kyba, C.C.M., Kuester, T., De Miguel, A.S., Baugh, K., Jechow, A., Hölker, F., Bennie, J., Elvidge, C.D., Gaston, K.J., Guanter, L., 2017. Artificially lit surface of Earth at night increasing in radiance and extent. Sci. Adv. 3, 1–9. https://doi.org/10.1126/sciadv.1701528.

Levin, N., 2017. The impact of seasonal changes on observed nighttime brightness from 2014 to 2015 monthly VIIRS DNB composites. Remote Sens. Environ. 193, 150–164. https://doi.org/10.1016/j.rse.2017.03.003.

Levin, N., Kyba, C.C.M., Zhang, Q., Sánchez de Miguel, A., Román, M.O., Li, X., Portnov, B.A., Molthan, A.L., Jechow, A., Miller, S.D., Wang, Z., Shrestha, R.M., Elvidge, C.D., 2020. Remote sensing of night lights: A review and an outlook for the future. Remote Sens. Environ. 237, 111443 https://doi.org/10.1016/j.rse.2019.111443.

Li, M., Koks, E., Taubenböck, H., van Vliet, J., 2020a. Continental-scale mapping and analysis of 3D building structure. Remote Sens. Environ. 245, 111859 https://doi.org/10.1016/j.rse.2020.111859.

Li, X., Zhao, L., Li, D., Xu, H., 2018. Mapping Urban Extent Using Luojia 1–01 Nighttime Light Imagery. Sensors 18, 1–18. https://doi.org/10.3390/s18113665.

Li, X., Gong, P., Zhou, Y., Wang, J., Bai, Y., Chen, B., Hu, T., Xiao, Y., Xu, B., Yang, J., Liu, X., Cai, W., Huang, H., Wu, T., Wang, X.i., Lin, P., Li, X., Chen, J., He, C., Li, X., Yu, L.e., Clinton, N., Zhu, Z., 2020b. Mapping global urban boundaries from the global artificial impervious area (GAIA) data. Environ. Res. Lett. 15 (9), 094044.

Li, X., Shang, X., Zhang, Q., Li, D., Chen, F., Jia, M., Wang, Y., 2022. Using radiant intensity to characterize the anisotropy of satellite-derived city light at night. Remote Sens. Environ. 271, 112920 https://doi.org/10.1016/j.rse.2022.112920.

Liao, L.B., Weiss, S., Mills, S., Hauss, B., 2013. Suomi NPP VIIRS day-night band on-orbit performance. J. Geophys. Res. Atmospheres 118, 12705–12718. https://doi.org/10.1002/2013JD020475.

Liu, S., Shi, K., Wu, Y., 2022. Identifying and evaluating suburbs in China from 2012 to 2020 based on SNPP–VIIRS nighttime light remotely sensed data. Int. J. Appl. Earth Obs. Geoinformation 114, 103041. https://doi.org/10.1016/j.jag.2022.103041.

Liu, Y., Wang, Z., Sun, Q., Erb, A.M., Li, Z., Schaaf, C.B., Zhang, X., Román, M.O., Scott, R.L., Zhang, Q., Novick, K.A., Syndonia Bret-Harte, M., Petroy, S., SanClements, M., 2017. Evaluation of the VIIRS BRDF, Albedo and NBAR products suite and an assessment of continuity with the long term MODIS record. Remote Sens. Environ. 201, 256–274. https://doi.org/10.1016/j.rse.2017.09.020.

Miller, S.D., Turner, R.E., 2009. A dynamic lunar spectral irradiance data set for NPOESS/VIIRS day/night band night time environmental applications. IEEE Trans. Geosci. Remote Sens. 47, 2316–2329. https://doi.org/10.1109/TGRS.2009.2012696.

Miller, S.D., Combs, C.L., Kidder, S.Q., Lee, T.F., 2012a. Assessing Moonlight Availability for Nighttime Environmental Applications by Low-Light Visible Polar-Orbiting Satellite Sensors. J. Atmospheric Ocean. Technol. 29, 538–557. https://doi.org/10.1175/JTECH-D-11-00192.1.

Miller, S.D., Mills, S.P., Elvidge, C.D., Lindsey, D.T., Lee, T.F., Hawkins, J.D., 2012b. Suomi satellite brings to light a unique frontier of nighttime environmental sensing capabilities. PNAS 109, 15706–15711. https://doi.org/10.1073/pnas.1207034109.

Ou, J., Liu, X., Liu, P., Liu, X., 2019. Evaluation of Luojia 1–01 nighttime light imagery for impervious surface detection: A comparison with NPP-VIIRS nighttime light data. Int. J. Appl. Earth Obs. Geoinformation 81, 1–12. https://doi.org/10.1016/j.jag.2019.04.017.

Polivka, T.N., Wang, J., Ellison, L.T., Hyer, E.J., Ichoku, C.M., 2016. Improving Nocturnal Fire Detection with the VIIRS Day-Night Band. IEEE Trans. Geosci. Remote Sens. 54, 5503–5519. https://doi.org/10.1109/TGRS.2016.2566665.

Román, M.O., Stokes, E.C., 2015. Holidays in lights: Tracking cultural patterns in demand for energy services. Earths Future 3, 182–205. https://doi.org/10.1002/2014EF000285.

Román, M.O., Wang, Z., Sun, Q., Kalb, V., Miller, S.D., Molthan, A., Schultz, L., Bell, J., Stokes, E.C., Pandey, B., Seto, K.C., Hall, D., Oda, T., Wolfe, R.E., Lin, G., Golpayegani, N., Devadiga, S., Davidson, C., Sarkar, S., Praderas, C., Schmaltz, J., Boller, R., Stevens, J., Ramos González, O.M., Padilla, E., Alonso, J., Detrés, Y., Armstrong, R., Miranda, I., Conte, Y., Marrero, N., MacManus, K., Esch, T.,

Masuoka, E.J., 2018. NASA's Black Marble nighttime lights product suite. Remote Sens. Environ. 210, 113–143. https://doi.org/10.1016/j.rse.2018.03.017.
Small, C., 2019. Multisensor characterization of urban morphology and network structure. Remote Sens 11 (18), 2162. https://doi.org/10.3390/rs11182162.
Tan, X., Zhu, X., Chen, J., Chen, R., 2022. Modeling the direction and magnitude of angular effects in nighttime light remote sensing. Remote Sens. Environ. 269, 112834 https://doi.org/10.1016/j.rse.2021.112834.
Wang, J., Aegerter, C., Xu, X., Szykman, J.J., 2016. Potential application of VIIRS Day/Night Band for monitoring nighttime surface PM2.5 air quality from space. Atmos. Environ. 124, 55–63. https://doi.org/10.1016/j.atmosenv.2015.11.013.
Wang, Z., Román, M.O., Kalb, V.L., Miller, S.D., Zhang, J., Shrestha, R.M., 2021. Quantifying uncertainties in nighttime light retrievals from Suomi-NPP and NOAA-20 VIIRS Day/Night Band data. Remote Sens. Environ. 263, 112557 https://doi.org/10.1016/j.rse.2021.112557.
Wang, J., Roudini, S., Hyer, E.J., Xu, X., Zhou, M., Garcia, L.C., Reid, J.S., Peterson, D.A., da Silva, A.M., 2020. Detecting nighttime fire combustion phase by hybrid application of visible and infrared radiation from Suomi NPP VIIRS. Remote Sens. Environ. 237, 111466 https://doi.org/10.1016/j.rse.2019.111466.
Xie, Y., Weng, Q., Fu, P., 2019. Temporal variations of artificial nighttime lights and their implications for urbanization in the conterminous United States, 2013–2017. Remote Sens. Environ. 225, 160–174. https://doi.org/10.1016/j.rse.2019.03.008.
Xu, G., Xiu, T., Li, X., Liang, X., Jiao, L., 2021. Lockdown induced night-time light dynamics during the COVID-19 epidemic in global megacities. Int. J. Appl. Earth Obs. Geoinformation 102, 102421. https://doi.org/10.1016/j.jag.2021.102421.
Yuan, M., Li, X., Li, D., Wu, J., 2022. An Analysis of Environmental Effect on VIIRS Nighttime Light Monthly Composite Data at Multiple Scales in China. IEEE J. Sel. Top. Appl. Earth Obs. Remote Sens. 16, 825–840. https://doi.org/10.1109/JSTARS.2022.3231960.
Zhang, J., Jaker, S.L., Reid, J.S., Miller, S.D., Solbrig, J., Toth, T.D., 2019. Characterization and application of artificial light sources for nighttime aerosol optical depth retrievals using the Visible Infrared Imager Radiometer Suite Day/Night Band. Atmospheric Meas. Tech. 12, 3209–3222. https://doi.org/10.5194/amt-12-3209-2019.
Zhao, X., Yu, B., Liu, Y., Yao, S., Lian, T., Chen, L., Yang, C., Chen, Z., Wu, J., 2018. NPP-VIIRS DNB daily data in natural disaster assessment: Evidence from selected case studies. Remote Sens. 10, 1–25. https://doi.org/10.3390/rs10101526.
Zhao, F., Zhang, S., Zhang, D., Peng, Z., Zeng, H., Zhao, Z., Jin, W., Shen, W., Liu, W., 2022. Illuminated border: Spatiotemporal analysis of COVID-19 pressure in the Sino-Burma border from the perspective of nighttime light. Int. J. Appl. Earth Obs. Geoinformation 109, 102774. https://doi.org/10.1016/j.jag.2022.102774.
Zhao, M., Zhou, Y., Li, X., Cao, W., He, C., Yu, B., Li, X.i., Elvidge, C.D., Cheng, W., Zhou, C., 2019. Applications of satellite remote sensing of nighttime light observations: Advances, challenges, and perspectives. Remote Sens. 11, 1971. https://doi.org/10.3390/rs11171971.
Zheng, Q., Weng, Q., Huang, L., Wang, K., Deng, J., Jiang, R., Ye, Z., Gan, M., 2018. A new source of multi-spectral high spatial resolution night-time light imagery — JL1-3B. Remote Sens. Environ. 215, 300–312. https://doi.org/10.1016/j.rse.2018.06.016.
Zheng, Q., Weng, Q., Wang, K., 2021. Characterizing urban land changes of 30 global megacities using nighttime light time series stacks. ISPRS J. Photogramm. Remote Sens. 173, 10–23. https://doi.org/10.1016/j.isprsjprs.2021.01.002.
Zheng, Q., Weng, Q., Zhou, Y., Dong, B., 2022. Impact of temporal compositing on nighttime light data and its applications. Remote Sens. Environ. 274, 113016 https://doi.org/10.1016/j.rse.2022.113016.
Zhu, X., Tan, X., Liao, M., Liu, T., Su, M., Zhao, S., Xu, Y.N., Liu, X., 2022. Assessment of a New Fine-Resolution Nighttime Light Imagery From the Yangwang-1 ("Look up 1") Satellite. IEEE Geosci. Remote Sens. Lett. 19, 1–5. https://doi.org/10.1109/LGRS.2021.3139774.